Molecular Architecture Effect on the Microphase Separations in Supramolecular Comb−Coil Complexes of Polystyrene-*block*-poly(2-vinylpyridine) with Dodecylbenzenesulfonic Acid: $(AB)_nA_n$ Block−Arm Star Copolymer

Bhanu Nandan,[†] Chia-Hua Lee,[‡] Hsin-Lung Chen,[*,†] and Wen-Chang Chen[*,‡,§]

Department of Chemical Engineering, National Tsing Hua University, Hsin-Chu 30013, Taiwan; Institute of Polymer Science and Engineering, National Taiwan University, Taipei 10617, Taiwan; and Department of Chemical Engineering, National Taiwan University, Taipei 10617, Taiwan

Received July 5, 2005; Revised Manuscript Received August 29, 2005

ABSTRACT: We studied the supramolecular comb−coil block copolymers formed by stoichiometric complexations of an amphiphilic surfactant, dodecylbenzenesulfonic acid (DBSA), with the poly(2-vinylpyridine) (P2VP) blocks in a linear polystyrene-*block*-poly(2-vinylpyridine) (PS-*b*-P2VP) and a nonlinear block−arm star copolymer of the type (PS-*b*-P2VP)$_5$PS$_5$. The effect of the block copolymer molecular architecture on the hierarchical structures in the ordered state and the relevant order−disorder transitions (ODT) have been revealed using small-angle X-ray scattering (SAXS). Both the linear and the block−arm complexes exhibited structure-within-structure morphology in which the larger-scale PS microdomains were embedded in the matrix consisting of the smaller-scale lamellar mesophase organized by the P2VP(DBSA) comb blocks. The order−disorder transition temperature (T_{ODT}) of the copolymer domain in the linear complex was significantly higher than that of neat PS-*b*-P2VP due to the stronger interblock repulsion caused by the increase in the polarity of P2VP blocks upon complexation with DBSA. In sharp contrast, the corresponding T_{ODT} of (PS-*b*-P2VP)$_5$(PS)$_5$(DBSA) complex was approximately the same as that of the neat copolymer. In this case the disruption of the PS microdomains induced a concurrent disordering of the smaller-scale lamellar mesophase because the entropic loss due to excessive stretching of short PS block chains in the microdomains overwhelmed the polar−nonpolar repulsion responsible for the formation of the lamellar mesophase. We have also observed a significant reduction in the interdomain spacing of the copolymer domains in the (PS-*b*-P2VP)$_5$(PS)$_5$(DBSA) complex compared to that in the neat copolymer. The smaller interdomain spacing was attributed to the lower aggregation number of PS star arms in the microdomains due to chain-crowding effect.

Introduction

Self-assemblies of block copolymer-based systems have attracted considerable attention in the area of nanotechnology which relies largely on the ability to arrange functional domains at the nanoscale. Block copolymers consisting of chemically different polymer chains form long-range ordered microdomain structures driven by the repulsive interaction between the constituent chains. The morphology depends on the volume ratio of the blocks, while the size of the structure, which is usually in the 10−100 nm range, is mostly influenced by the lengths of the blocks. The typical morphological patterns observed for linear coil−coil diblock copolymers include body-centered-cubic (bcc) packed spheres, hexagonally packed cylinders, and 1-D stacked alternating lamellae.[1−9] Similar to block copolymers are polymers with comb-shaped architecture which tend to self-organize in an essentially similar way.[10] In comb-shaped polymers, the covalent bonding between the backbone and the repulsive side chains may be replaced by the weaker physical interactions such as ionic bonds, hydrogen bonds, and metal-mediated coordination bonds to form supramolecules which may analogically self-organize to form mesomorphic nanostructures.[11−23]

Recently, polymers with hierarchical structures have been drawing significant interest due to their potential use as functional materials in electrical, optical, and other functionalities.[24−36] The self-organized domains at multiple length scales offer switchlike controls of material functionalities by the relevant order−disorder or order−order transitions. A simple way to construct these hierarchical structures is by combining the concept of self-assembly in block copolymers involving covalent bonds and that in supramolecular comb polymers involving physical interactions. The basic strategy involves the selective grafting of one of the repulsive blocks of the copolymer with the short-chain amphiphilic molecules through noncovalent interactions, resulting in the so-called supramolecular comb−coil block copolymers.[21] In this case, the microphase separation driven by the incompatibility between the comb and coil blocks yields the copolymer domains of several tens of nanometers, and the polar−nonpolar repulsion between the backbone and the side chains of the comb block induces the formation of a lamellar mesophase with a characteristic length of several nanometers. The phase transition temperatures of the lamellar mesophase may be tailored by the strength of the secondary interaction holding up the comb architecture. Ionic bonding normally results in an order−disorder transition (ODT) temperature (T_{ODT}) close to or even above the thermal decomposition temperature of the system, while T_{ODT} becomes well below the thermal degradation temperature for the weaker binding forces such as hydrogen bonds.

[†] National Tsing Hua University.
[‡] Institute of Polymer Science and Engineering, National Taiwan University.
[§] Department of Chemical Engineering, National Taiwan University.
* To whom correspondence should be addressed.

10.1021/ma051448t CCC: $30.25
Published on Web 11/01/2005

The supramolecular comb−coil concept was pioneered and widely studied by Ikkala and co-workers.[15,21,25−33,35,36] The best studied example involved a linear diblock copolymer of polystyrene (PS) and poly(4-vinylpyridine) (P4VP) with the amphiphile pentadecylphenol (PDP) hydrogen bonded stoichiometrically to the P4VP blocks. Usually, a microphase-separated morphology consisting of PS and P4VP(PDP) domains was present throughout the experimental temperature range (0−250 °C) with a characteristic length scale on the order of 10−50 nm. Under stoichiometric conditions the smaller-scale structure organized by the comb-shaped P4VP(PDP) blocks was formed inside the P4VP(PDP) domains below ca. 65 °C, thereby leading to structure-within-structure morphology. Lamellae-within-lamellae, lamellae-within-cylinder, and lamellae-within-sphere as well as the complementary structures have all been demonstrated.[15,24,25] In a slightly more complicated example, P4VP was first protonated with a strong acid such as methanesulfonic acid (MSA) to which PDP was subsequently hydrogen bonded, leading to PS-*b*-P4VP(MSA)(PDP) complexes.[15,27,29,31] The presence of MSA increased the ODT of the smaller-scale structure to 100 °C. This kind of complex can also be used to prepare materials with reversible switching band gaps. In the case of high molar mass PS-*b*-P4VP diblock copolymers, it has been shown that the PS-*b*-P4VP(DBSA) supramolecules, where DBSA denotes dodecylbenzenesulfonic acid, formed self-assembled one-dimensional optical reflectors.[30] Recently, we have shown that in the case of poly(1,4-butadiene)-*block*-poly(ethylene oxide) (PB-*b*-PEO) diblock copolymer complexed with DBSA, in addition to the structure-within-structure morphology, the supramolecular comb−coil diblock exhibited a transition-driven transition through which the morphology of the larger-scale copolymer domain was switched by the ODT of the smaller-scale assembly of the comb block.[34] Ikkala and co-workers have also reported several order−order transitions observed as a function of temperature in the case of 1,4-polyisoprene-*block*-poly(2-vinylpyridine) complexed with octyl gallate (OG).[33,36] The absence of hydrogen bonding between the octyl gallate molecules and the pyridine groups at elevated temperatures was argued to be the key factor for many of the observed phenomena in these complexes.[33] This showed that the nature of self-assembly of these supramolecular comb−coil systems near the ODT of the comb block can be highly complex and still has to be fully understood.

The supramolecular comb−coil concept used for designing materials with hierarchical structures until now has been applied only to the complexes of linear diblock copolymers. Their phase behavior at ambient conditions has been well understood. In the present study, we focus our attention on the supramolecular comb−coil complexes of an amphiphilic surfactant with a nonlinear block copolymer. The most commonly known nonlinear block copolymers are A_nB_n heteroarm star copolymers which are constituted of a central core bearing arms of pure polymer A and pure polymer B and $(AB)_n$ type block−arm star copolymers having several diblocks junctioned on a common core. These special macromolecular architectures are challenging not only from synthesis point of view but also as a promising way to modulate the free energy balance and thus the phase structures of block copolymers.[37−40] Like linear diblock copolymers, these polymeric species undergo microphase separation to form well-ordered structures. On the other hand, the difference in architecture between star and linear copolymers results naturally in much slower phase separation kinetics and modification of the equilibrium structures.[4,9,41−49] In the block−arm star copolymers, the tendency of the core block to locate inside the cylindrical and spherical microdomains leads to an asymmetry in the phase diagram whereas in the case of heteroarm star copolymers the difference in the number of arms of the two blocks causes an asymmetry in the phase diagram compared to that of the corresponding linear diblock. Hence, the supramolecular comb−coil complexes of these star copolymers may also show different phase behavior compared to their linear counterpart and may result in interesting and anomalous self-organized structures and phase transitions.

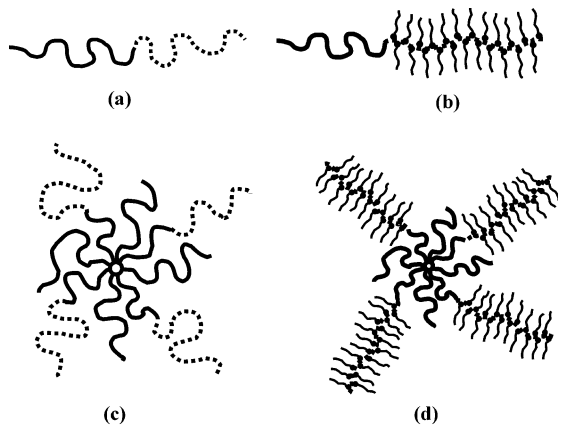

Figure 1. Schematic representation of the molecular architecture of the block copolymers and their complexes studied: (a) linear PS-*b*-P2VP diblock copolymer; (b) linear PS-*b*-P2VP diblock copolymer complexed with surfactant; (c) block−arm star copolymer of the type $(PS\text{-}b\text{-}P2VP)_nPS_n$; (d) block−arm star copolymer of the type $(PS\text{-}b\text{-}P2VP)_nPS_n$ complexed with a surfactant. The PS blocks are directly attached to the core of the star copolymer whereas P2VP(DBSA) blocks are located away from the central core. The actual number of arms in the star copolymer used in this study is more than that shown in the figure.

The objective of this paper is to investigate how the molecular architecture influences the self-assembled structure and phase transitions of supramolecular comb−coil block copolymers. Here we deal with a $(AB)_nA_n$ kind of block−arm star copolymer which consists of several A chains junctioned at the common junction point of simple $(AB)_n$ block−arm star copolymer. The case of the complexes consisting of A_nB_n heteroarm star copolymer will be discussed elsewhere.[50] The system under study is the complex of $(PS\text{-}b\text{-}P2VP)_5(PS)_5$ block−arm star copolymer with an amphiphilic surfactant, DBSA. For comparison, a linear PS-*b*-P2VP(DBSA) complex with equivalent composition is also studied here. A schematic of the chain architecture of the block copolymers together with their supramolecular comb−coil complexes investigated in the present study is shown in Figure 1.

Our approach is twofold. First, we study the self-assemblies of the neat block copolymers. The molecular architecture effect on the microphase separation behavior in neat $(PS\text{-}b\text{-}P2VP)_5(PS)_5$ will be compared with that reported in the literature for the simpler $(AB)_n$ block−arm star copolymer. It is noted that here we use block copolymers of lower molecular weights, which makes it possible to access their ODT's. This in turn allows us to reveal the architecture influence on the temperature

Scheme 1

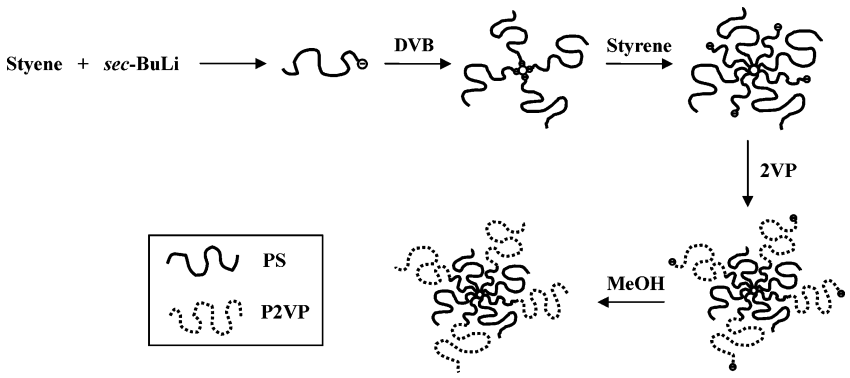

Table 1. Molecular Characteristics of Polystyrene/Poly(2-vinylpyridine) Linear and Block−Arm Star Copolymers

sample[a]	M_w[b] overall	M_w[c] PS arm	M_w[d] PS arm	M_w[e] P2VP arm	M_w/M_n	N[f]	f_{PS}[g]	f_{PS}[h]
BA	55950	1150	3480	6760	1.3	4.9	0.41	0.14
LA	8790	4480		4310	1.1		0.51	0.20

[a] "BA" represents block−arm star copolymer, and "LA" represents linear diblock copolymer. [b] Weight-average molecular weight of the whole macromolecule. [c] Weight-average molecular weight of PS block in a single diblock arm. [d] Weight-average molecular weight of a free PS arm in the block−arm star copolymer. The number of such arms in one macromolecule is same as the number of diblock arms. [e] Weight-average molecular weight of P2VP block in a single diblock arm. [f] Average functionality, i.e., average number of PS-*b*-P2VP arms in the star copolymer. [g] Overall volume fraction of PS in the neat copolymer. [h] Overall volume fraction of PS in the copolymers after complexation with DBSA.

dependence of the self-assembled structures. Then we proceed to study the microphase separations in the complexes of the block copolymers with DBSA. We will show that hierarchical structures with two distinct length scales were formed irrespective of the architectural complexity of the constituting block copolymers. One interesting aspect we will focus here is the interplay between the ODT's associated with the structures of the two length scales. The disordering of the larger-scale copolymer domains into a homogeneous melt has to induce the disordering of the smaller lamellar structure formed by the comb blocks, while that of the smaller-scale structure may give rise to some interesting transformations of the morphology of the copolymer domains.[33,34,36] Here we will direct significant attention to the molecular architecture influence on the coupling of the two ODT's in the supramolecular comb−coil complexes under study.

Experimental Section

Synthesis and Characterization of Neat Block Copolymers. The linear PS-*b*-P2VP block copolymer was synthesized by sequential living anionic polymerization of styrene monomer followed by 2-vinylpyridine monomer as described elsewhere.[51] The $(AB)_nA_n$ type of PS−P2VP block−arm star copolymer was synthesized by the sequential anionic living polymerization similar to the star block P2VP-*block*-poly(*tert*-butyl acrylate) copolymer reported in the literature,[52] as shown in Scheme 1. First some living PS arms were synthesized using *sec*-butyllithium as the initiator. The reaction temperature was maintained at −78 °C. Then, the monomers of divinylbenzene (DVB), styrene, and 2-vinylpyridine (2-VP) were added in sequence. The living anionic polymerization was terminated by methanol, precipitated in hexane, and then filtered out to obtain the polymer product. The block copolymer samples were subsequently purified by fractionation and characterized by ^{1}H NMR and gel permeation chromatography (GPC). The detailed molecular characteristics of the copolymer samples are given in Table 1. The linear PS-*b*-P2VP (LA in Table 1) had a weight-average molecular weight (M_w) of 8790 with a low polydispersity index of 1.1, and the volume fractions of PS in the neat copolymer and the complex with DBSA were 0.51 and 0.20, respectively. The block−arm star PS-*b*-P2VP (BA in Table 1) had a M_w of 55 950 with a polydispersity index of 1.3, and the volume fractions of PS in the neat copolymer and the complex were 0.41 and 0.14, respectively. The average number of block arms in BA was 4.9; therefore, the copolymer was denoted as $(PS\text{-}b\text{-}P2VP)_5PS_5$.

Complex Preparation. The block copolymers and DBSA were first dissolved in THF separately to form clear solutions. The complexes with binding fraction $x = 1.0$ were then prepared by combining appropriate quantity of the two solutions. The binding fraction represents the average number of DBSA molecules bound with a P2VP monomer unit. The solution was stirred for 24 h followed by slowly evaporating the solvent at room temperature. The samples were finally dried in a vacuum at 60 °C for 2 days to remove the residual solvent.

SAXS Measurements. SAXS measurements were performed using a Bruker Nanostar SAXS instrument. The X-ray source, a 1.5 kW X-ray generator (Kristalloflex 760) equipped with a Cu tube, was operated at 35 mA and 40 kV. The scattering intensity was detected by a two-dimensional position-sensitive detector (Bruker AXS) with 512 × 512 channels. The area scattering pattern has been radially averaged to increase the photon counting efficiency compared with the one-dimensional linear detector. The intensity profile was output as the plot of the scattering intensity (I) vs the scattering vector, $q = 4\pi/\lambda \sin(\theta/2)$ (θ = scattering angle). All scattering data were corrected by the empty beam scattering, the sensitivity of each pixel of the area detector, and thermal diffuse scattering (I_{TDS}). The thermal diffuse scattering was considered as a positive deviation from the Porod law[53,54] and may be associated with thermal motion, local disorder, or frozen-in fluctuations. I_{TDS} can be regarded as a constant background, and the total scattered intensity in the high-q region is expressed by the Porod−Ruland equation[55]

$$I(q) = \frac{K_P \exp(-\sigma^2 q^2)}{q^4} + I_{TDS} \quad (1)$$

where K_P is the Porod's constant and σ is a parameter related to the thickness of interphase for a two-phase structure. The exponential term in eq 1 becomes insignificant at sufficiently high q such that a plot of $I(q)q^4$ vs q^4 would yield a straight line with a slope given by I_{TDS}. Temperature-dependent SAXS measurements were performed under vacuum at the accuracy of temperature control of ±0.2 °C. The sample was first

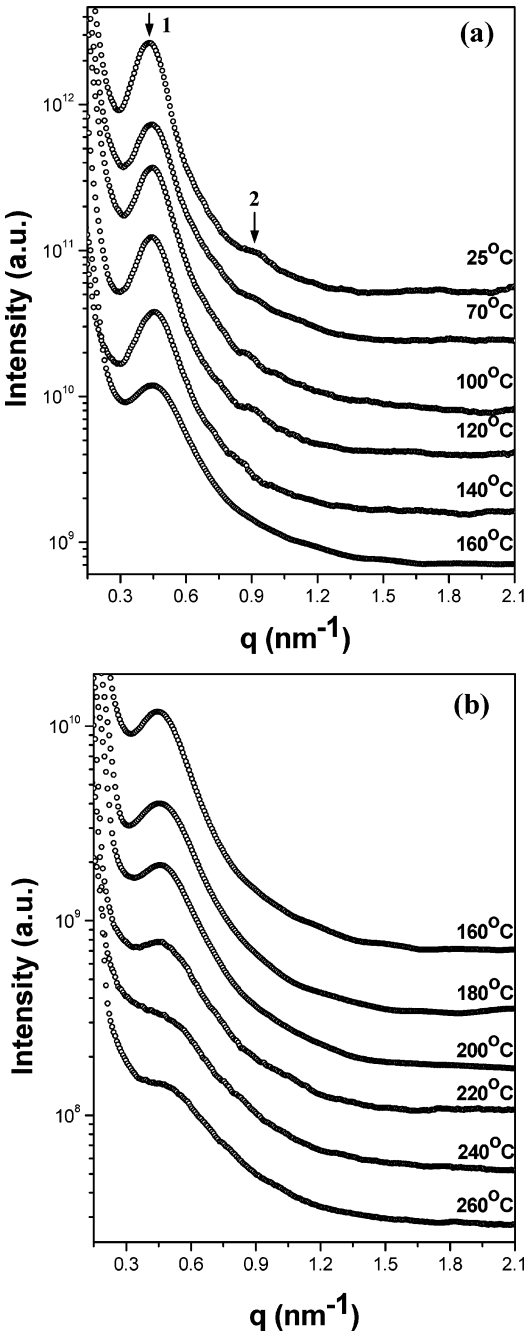

Figure 2. Temperature-dependent SAXS intensity profiles of neat LA diblock copolymer collected in situ from (a) 25 to 160 °C and (b) 160 to 260 °C in a heating cycle.

equilibrated at the measuring temperature for 20 min followed by 1 h data acquisition.

Results and Discussion

Self-Assemblies and ODT's of the Neat Block Copolymers. For the convenience of presentation, we will denote the linear PS-*b*-P2VP by "LA" and the (PS-*b*-P2VP)$_5$(PS)$_5$ block−arm star copolymer by "BA". Figure 2a,b shows the temperature-dependent SAXS profiles of neat LA copolymer obtained in-situ in the temperature range of 25−260 °C. The SAXS profiles at low temperatures showed a relatively sharp primary scattering maximum at 0.44 nm^{-1} and a faint second-order peak near 0.88 nm^{-1}, indicating the formation of a lamellar morphology consisting of alternating PS and P2VP lamellae. This morphological structure was expected considering the composition of the diblock copolymer (i.e., the volume fraction of PS, $f_{PS} = 0.51$). The interlamellar distance at 25 °C as calculated using the Bragg's equation ($D = 2\pi/q_m$ with q_m being the position of the primary diffraction peak) was 14.27 nm. As the temperature increased, the intensity of the primary peak decreased along with a peak broadening. A sharp and remarkable change in the scattering pattern was clearly discerned between 140 and 160 °C due to the occurrence of ODT. The broad peak observed in the disordered state has been attributed to the so-called "correlation hole" effect which reflects the concentration fluctuations of the block copolymer segments in the single phase state.[1,56] The peak scattering vector here is related to the characteristic wavelength of the dominant mode of the concentration fluctuations.

The abrupt change of the scattering pattern across the ODT enables the determination of the T_{ODT}. There are different ways, based on the mean-field theory, for locating T_{ODT} from the SAXS results. Two of the common methods are use of the plots of (i) the reciprocal of the maximum scattered intensity (I_m^{-1}) vs the reciprocal of the absolute temperature (T^{-1}) and (ii) D ($= 2\pi/q_m$) vs T^{-1}. According to Leibler's mean-field theory,[1] I_m^{-1} is expected to decrease linearly with T^{-1} in the disordered state, i.e.

$$I_m^{-1} \sim a - b/T \tag{2}$$

where a and b are positive constants. Equation 2 assumes that the temperature dependence of the Flory−Huggins segmental interaction parameter between the block chains (χ_{A-B}) is given by

$$\chi_{A-B} = A + B/T \tag{3}$$

where A and B are constants. Moreover, Leibler's theory[1] predicts that D or q_m in the disordered state is essentially independent of temperature, if we omit the small temperature variation originating from the temperature dependence of the radius of gyration of block chains, $R_g(T)$, i.e.

$$D/R_g(T) \sim T^0 \tag{4}$$

Thus, in the context of the mean-field theory, the deviation in the temperature dependence of I_m^{-1} from eq 2 and the deviations in the temperature dependence of D from eq 4 are ascribed to an onset of the disordering process on heating and hence may be utilized for determination of the T_{ODT}. Figure 3 presents the plots of I_m^{-1} and D vs T^{-1} for the LA copolymer. A linear decrease of I_m^{-1} in the disordered state and almost constant value in the low-temperature range (ordered state) were observed, which was consistent with the theoretical predictions. The crossover of I_m^{-1} vs T^{-1} showed that the T_{ODT} was located at ca. 150 °C. D was found to increase abruptly upon raising the temperature across the ODT. This result is particularly interesting since in most cases D has been reported to show a discontinuous decrease on raising the temperature across ODT. However, there have been few reports where such discontinuous increase in D has been observed though no definite explanation has been given. Hashimoto et al.[57] observed similar behavior in a cylinder-forming polystyrene-*block*-polyisoprene (PS-*b*-PI) block copolymer and they suggested that it may be due to a symmetry break from a superposition of plane

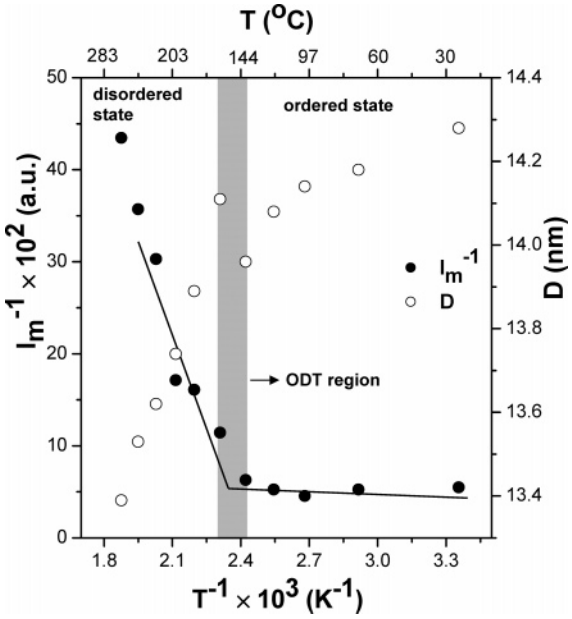

Figure 3. I_m^{-1} and D vs T^{-1} plot of neat LA diblock copolymer for T_{ODT} determination.

wave fluctuations (in the disordered state) to hexagonal symmetry of cylinders (in the ordered state). Floudas et al.[41] have also reported a similar variation of the scattering maximum with T^{-1} in the case of a heteroarm star copolymer.

Next we analyze the phase behavior of neat (PS-*b*-P2VP)$_5$PS$_5$ block−arm star copolymer (i.e., BA). Figure 4a,b shows the temperature-dependent SAXS profiles of BA obtained in the temperature range of 25−240 °C. The SAXS profile at room temperature showed a sharp primary scattering peak at $q = 0.43$ nm^{-1} along with weak second- and third-order peaks, signaling the formation of a lamellar morphology. The lamellar morphology was the most plausible since the composition of the copolymer was close to symmetric ($f_{PS} = 0.41$). It is noted that the block copolymers used in this study had low molecular weights and hence highly ordered self-assembled structures which gave rise to well-defined lattice peaks in the SAXS profile may not be observed here. The interlamellar distance at room temperature was found to be 14.60 nm, which was slightly greater than that of LA copolymer. As the temperature increased, the intensity and breadth of the first-order maximum showed a significant change from 140 to 160 °C, which again revealed the occurrence of an ODT. The ODT was more clearly revealed from the plots of I_m^{-1} and D vs T^{-1} shown in Figure 5. A significant drop in the intensity was observed on heating to 160 °C which showed that T_{ODT} of neat BA copolymer was located near this temperature. Moreover, the plot of D vs T^{-1} also showed a sharp change as the temperature was raised above 140 °C. Furthermore, the increase of D with increasing temperature observed in the ordered state was quite unusual and may be due to the star molecular architecture of the copolymer. The exact origin of this phenomenon is not clear at present.

The observed T_{ODT} of neat BA was close to that observed for neat LA copolymer. However, as will be discussed now, the simple $(AB)_n$ block−arm star copolymer should exhibit a higher T_{ODT} than the linear AB diblock copolymer with the same composition and molecular weight. A theory of microphase separation thermodynamics for graft and star copolymers has been

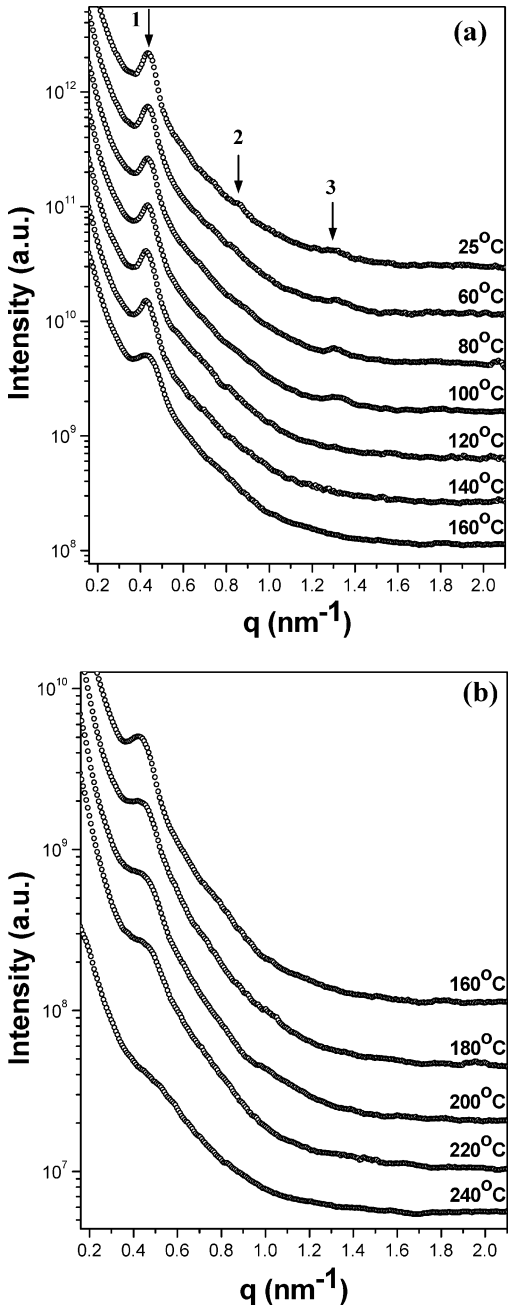

Figure 4. Temperature-dependent SAXS intensity profiles of neat BA star copolymer collected in situ from (a) 25 to 160 °C and (b) 160 to 240 °C in a heating cycle.

developed by de la Cruz and Sanchez.[37] The theory predicted striking differences between the phase behavior of linear diblock copolymers and that of graft and star copolymers. Here, we mainly concern with the predicted behavior in $(AB)_n$ block−arm star diblock copolymers which is close in architecture to the $(AB)_nA_n$ type block−arm copolymer used in this study. According to the mean-field theory of de la Cruz and Sanchez,[37] a lowering of the transition entropy was expected in the case of star blocks because of the junction constraint. The transition entropy change for a block−arm star copolymer, ΔS, is proportional to

$$\Delta S \sim \Delta S_0 - [(n-1)/n] \ln(1/f) \qquad (5)$$

where ΔS_0 refers to the transition entropy change in the case of a simple linear diblock and f is the fraction

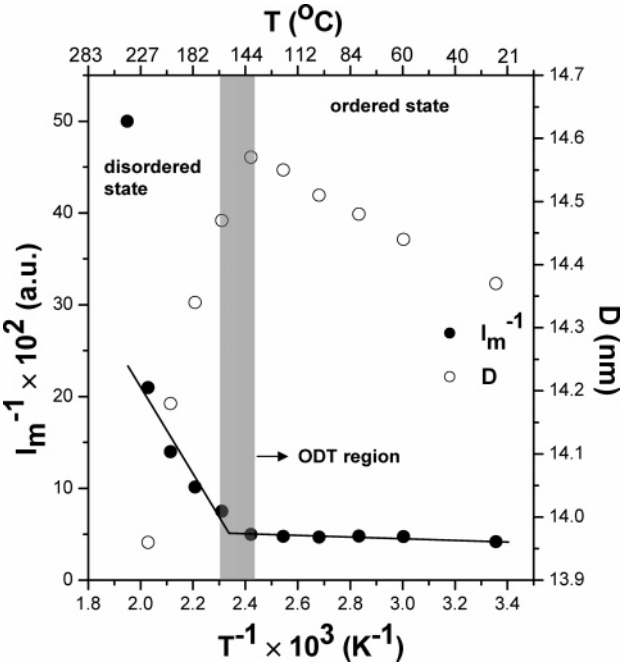

Figure 5. I_m^{-1} and D vs T^{-1} plot of neat BA star copolymer for T_{ODT} determination.

of A monomers in the copolymer. Since $(\chi N_0)_s$, where χ is the Flory–Huggins interaction parameter and N_0 is the number of monomers in one arm of the star copolymer, is proportional to the transition entropy, the expectation is that the spinodal will be smaller than that for a linear diblock copolymer. According to this theory, for $f = 0.5$, $(\chi N_0)_s$ is equal to 10.5, 8.86, and 7.07 for $n = 1$, 2, and 4, respectively. Hence, the T_{ODT} of a $(AB)_n$ block–arm star diblock is expected to be higher than that of the linear diblock of equivalent block molecular weight and composition. These theoretical predictions have been supported well by the experimental findings of Floudas et al.[42] and Hashimoto et al.[58]

In the present system we found that the T_{ODT} of linear PS-*b*-P2VP and block–arm (PS-*b*-P2VP)$_5$(PS)$_5$ star copolymer was almost same. Thus, the T_{ODT} of the block–arm star copolymer with the architecture of $(AB)_nA_n$ type is significantly lower than that of simple $(AB)_n$ type. Let us understand why it was so by looking at the chain conformation of PS blocks in the lamellar microdomains of the neat BA block–arm star copolymer. Figure 6a proposes a schematic representation of the chain arrangement in the lamellar domains. The block–arm star copolymer used in the present study had several longer free PS arms (shown in light gray) unconnected with P2VP blocks joined at the common star junction point apart from the short PS chains of the diblock arm. The molecular weight of these free PS arms was almost 3 times that of the short PS diblock arms. The extensive lateral chain crowding near the star junction point necessitated the stretching of the longer free PS chains away from the star junction point and, in this case, normal to the microdomain interface. To accommodate the longer PS chains within the PS lamellar microdomains, the shorter PS chains (shown in dark) may also need to stretch considerably to reach at the domain interface. The significant stretchings of the PS chains resulted in sizable loss in conformational entropy and hence increased the free energy of the system in the ordered state. Hence a lower T_{ODT} for $(AB)_n(A)_n$ type of block–arm star copolymer was expected compared to the simple $(AB)_n$ type copolymer of similar composition.

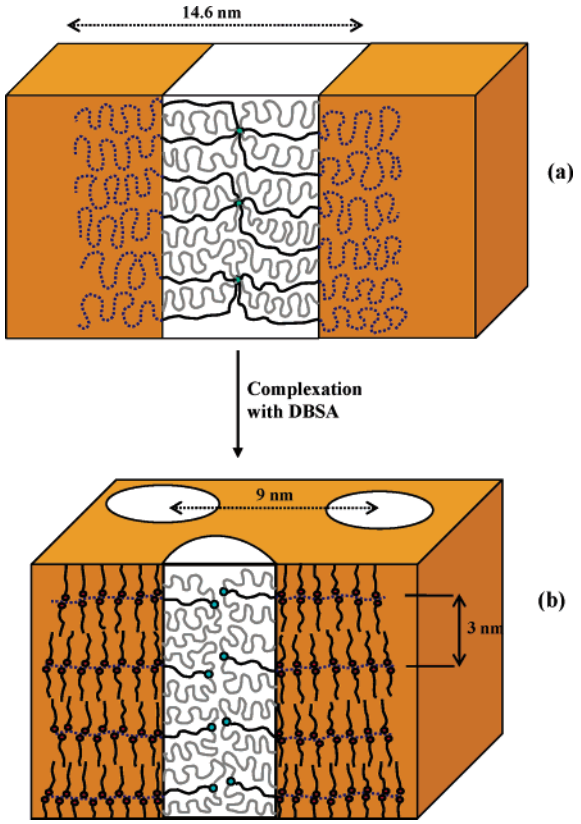

Figure 6. Schematic illustration of chain conformations of the block chains in (a) neat BA star copolymer having lamellar morphology and (b) BA(DBSA) comb–coil complex having cylindrical microdomains of PS embedded in the lamellar mesophase formed by P2VP(DBSA) comb blocks. The free PS chains are depicted in gray whereas the PS chains of diblock arms are shown in dark. The crowding effect at the junction point of star copolymer drives the stretching of both the longer free PS arms and the shorter PS chains of the diblock arms normal to the domain interface, resulting in an entropic loss. The actual number of arms in the star copolymer used in this study is more than that shown in the figure.

Hierarchical Structures and ODT's of the Comb–Coil Complexes. The phase behavior of the supramolecular comb–coil complexes was investigated using SAXS. Figure 7a,b shows the temperature-dependent SAXS profiles of the LA(DBSA) complex. The SAXS profile at room temperature showed a rather weak first-order scattering maximum at $q = 0.28$ nm^{-1} and a broad shoulder (marked by "$i = 1$") at $q \sim 0.58$ nm^{-1}. Another peak of strong intensity was observed in the high-q region at $q = 2.07$ nm^{-1}. The SAXS peaks in the low-q region were associated with the larger-scale structure due to microphase separation between PS and P2VP(DBSA) blocks. On increasing the temperature, the two low-q peaks became more intense. At 240 °C the higher-order scattering peaks associated with the long-range order of the copolymer domains became visible (Figure 7b). The lattice scattering was even clearer in the SAXS profile of the 240 °C-annealed sample collected using synchrotron radiation source (see Supporting Information). The positions of the lattice peaks closely followed the ratio of $1:3^{1/2}:4^{1/2}:7^{1/2}$, corresponding to a hexagonally packed cylinder structure. Therefore, the system contained hexagonally packed PS cylinders dispersed in the P2VP(DBSA) matrix as PS was the minor component with the volume fraction of 0.20.

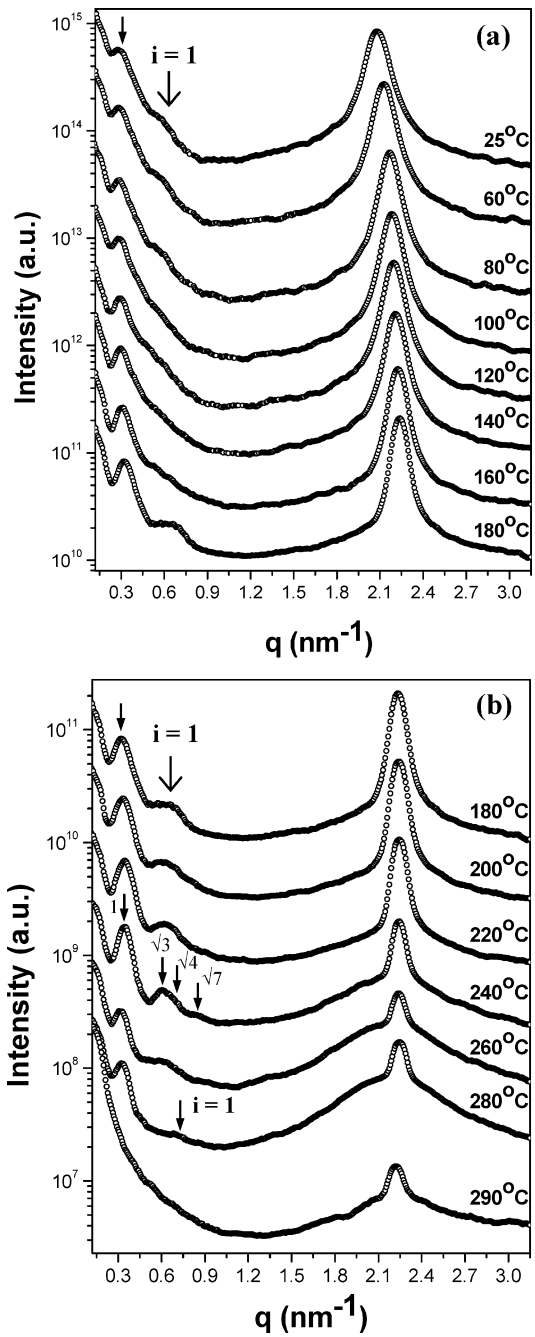

Figure 7. Temperature-dependent SAXS intensity profiles of LA(DBSA) comb−coil complex collected in-situ from (a) 25 to 180 °C and (b) 180 to 290 °C in a heating cycle.

The long-range order of the PS cylinders was not attained in the as-cast state as the corresponding SAXS profile only showed a broad scattering peak at 0.28 nm^{-1} (corresponding to the interdomain distance of 22.4 nm) (cf. Figure 7a). The shoulder marked by "$i = 1$" was attributed to the first-order form factor maximum ($q_m^{i=1}$) of the PS cylindrical domains. The average radius of the PS cylinders deduced from the form factor peak position via $R = 4.98/q_m^{i=1}$ was 8.6 nm. The positional order of the PS cylinders was enhanced upon heating, and the equilibrium hexagonal lattice was attained near 240 °C. On further heating the intensities of the lattice peaks decreased, and the scattering profile in the low-q region became similar to that observed for the as-cast state at 25 °C (cf. Figure 7b). Hence, a thermal fluctuation-driven lattice disordering took place between 240 and 260 °C, where the packing of PS cylinders became short-range ordered. The primary peak shifted to higher q and became sharper when the temperature was further increased to 280 °C. The form factor peak was also found to shift to higher q. It will be shown latter that the smaller-scale lamellar mesophase organized by P2VP(DBSA) blocks was mostly disrupted at this temperature. In this case, LA(DBSA) may be regarded as a simple mixture of LA with a selective solvent (DBSA), and PS domains may have transformed into spheres judging from the PS volume fraction of 0.20.

When the system finally reached 290 °C, the primary scattering maximum as well as the form factor peak vanished from the SAXS profile. This indicated that the system attained a micelle-free disordered state in which the PS and P2VP(DBSA) block chains mixed on a segmental level. The absence of a correlation hole peak suggested that thermal degradation might also have occurred at such a high temperature. Nevertheless, it was clear from the temperature-dependent SAXS experiment that T_{ODT} of the copolymer domain structure in LA(DBSA) complex was higher than 280 °C. Hence, the T_{ODT} of LA copolymer was raised by more than 120 °C upon complexation with DBSA. This significant increase of T_{ODT} was attributable to the increase of the polarity of P2VP blocks on complexation with DBSA because of the presence of ionic moiety. Hence, the repulsion between the polar P2VP(DBSA) units and the nonpolar PS blocks was stronger compared to that between P2VP and PS blocks, i.e., $\chi_{PS-P2VP(DBSA)} > \chi_{PS-P2VP}$.

We now turn to the temperature dependence of the high-q scattering peak located at 2.07 nm^{-1}. This peak was attributed to the primary diffraction maximum from the smaller-scale lamellar structure (with an interlamellar distance of 3.0 nm) organized by the P2VP(DBSA) comb blocks. The sharpness of the scattering peak as well as the fact that the intensity in the tail region obeyed approximately the Porod's law of $I(q) \sim q^{-4}$ (indicating a well-defined interface between two microphases) ruled out the possibility that it was a correlation hole peak due to dynamic thermal concentration fluctuations. The formation of the lamellar mesophase was further evidenced from the mesomorphic birefringent pattern observed under polarized optical microscopy (POM) (see Supporting Information). Hence, the LA(DBSA) comb−coil complex self-organized into a cylinder-within-lamellae morphology. The morphology of LA diblock copolymer before and after complexation with DBSA is schematically illustrated in parts a and b of Figure 8, respectively.

As can be seen in Figure 7b, the intensity of the P2VP(DBSA) lamellar peak dropped drastically as the temperature was increased to 220 °C, where the residual lamellar peak was found to superpose with a broad halo. The broad halo grew with increasing temperature at the expense of the sharp lamellar peak. The temperature-dependent SAXS profiles clearly revealed an ODT from the lamellar mesophase to a disordered phase in which the persistence of comb structure gave rise to a broad correlation hole peak. The T_{ODT} range of the P2VP(DBSA) lamellar mesophase was assessed from Figure 9, which shows a plot of I_m^{-1} vs T^{-1}. The T_{ODT} thus estimated was about 220 °C. This T_{ODT} agreed well with the temperature at which the mesomorphic birefringent pattern observed under POM disappeared.

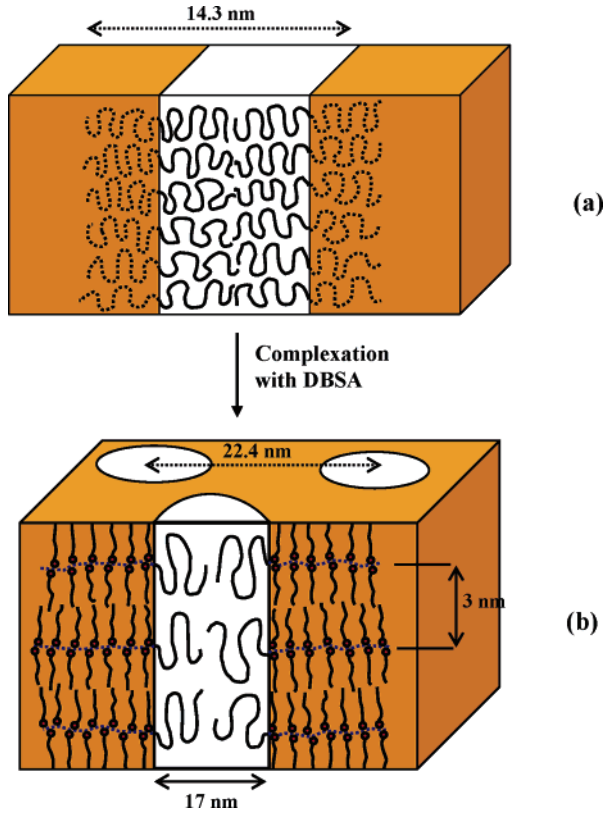

Figure 8. Schematic illustrations of the (a) lamellar morphology formed in neat LA copolymer and (b) hierarchical structure formed in LA(DBSA) complex where cylindrical microdomains of PS are embedded in the lamellar mesophase formed by P2VP(DBSA) comb blocks.

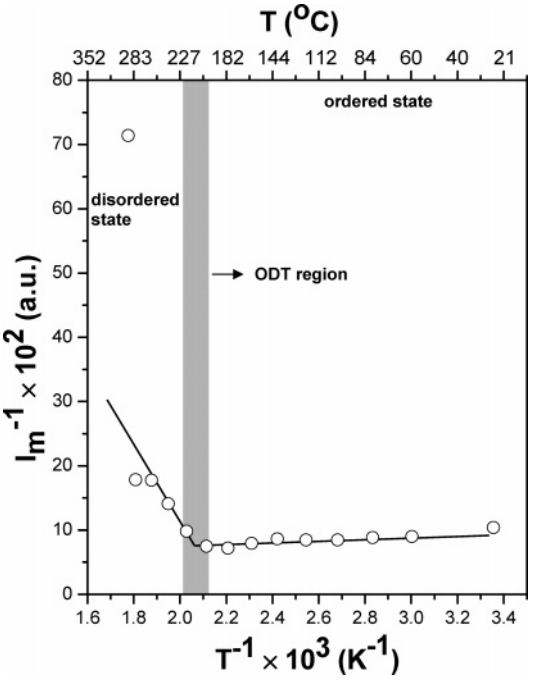

Figure 9. I_m^{-1} and D vs T^{-1} plot of LA(DBSA) complex for determination of T_{ODT} associated with P2VP(DBSA) comb blocks.

It is noted that DBSA attached to the P2VP blocks via both ionic and hydrogen bonding, with the latter being more predominant (see Supporting Information for more detail). The observed ODT of the lamellar mesophases may stem only from the dissociation of the weaker hydrogen bonds; namely, the ionically bonded DBSA remained intact even after the observed ODT has been reached. This was indeed revealed from Figure 7b where a weak sharp scattering peak was found to superimpose on a broad correlation hole peak even after the T_{ODT}, indicating the presence of residual lamellar domains. These lamellar domains were formed by the P2VP(DBSA) comb blocks with DBSA ionically bonded to P2VP.

In light of the observations that the copolymer domains did not undergo ODT until at least 280 °C and the P2VP(DBSA) lamellar mesophase disordered near 220 °C, it was concluded that the smaller-scale lamellar mesophase in LA(DBSA) complex disordered prior to the larger-scale copolymer microdomains. Once the T_{ODT} of the P2VP(DBSA) domains had been reached, the dissociated DBSA simply became a selective solvent for P2VP blocks such that an order−order transition (OOT) transforming the PS domains from cylinder to the more stable spherical domain might occur at 280 °C, as was discussed previously.

Figure 10a,b shows the temperature-dependent SAXS profiles of BA(DBSA) complex. At room temperature the SAXS profile consisted of a primary peak at 0.69 nm^{-1} and another intense peak at 2.08 nm^{-1}. The low-q peak again represented the larger-scale morphology formed by the microphase separation between PS and P2VP(DBSA) blocks (with an interdomain distance of 9.1 nm), whereas the high-q peak was ascribed to the lamellar structure within the P2VP(DBSA) domains (with an interlamellar distance of 3.0 nm). This showed that despite the complex architecture of BA star copolymer, the BA(DBSA) complex also self-organized on multiple length scales. Since the volume fraction of PS block in BA(DBSA) complex was 0.14, we might expect a morphology of bcc-packed PS spheres dispersed in the matrix constituting of the comb blocks. However, the absence of the higher-order peaks indicated that the packing of PS domains lacked long-range order. In this case the PS microdomain was most likely to have a cylindrical structure since it would be easier for the P2VP(DBSA) lamellar array around a PS cylinder to extend over a long distance once the polar/nonpolar layers stacked along the cylinder long axis.[34]

Another interesting observation to note here is that the primary scattering peak due to the copolymer domains was located at significantly higher q than that observed for neat BA star copolymer, indicating a much shorter characteristic interdomain spacing (= 9.1 nm) in the complex than that (= 14.6 nm) in neat BA. This was plausible since the cylindrical microdomain size in the BA(DBSA) complex was determined by the aggregation number of the star macromolecules. It had been reported that in selective solvent the block−arm star copolymers tended to form micelles of smaller size, having lower aggregation number and shorter coronas compared to the linear diblock.[59] This behavior was explained on the ground that more arms a star copolymer possesses the greater the difficulty to accommodate itself in a micelle due to excluded-volume effects as well as the elastic energy loss of the soluble arms.[59] Hence, the chain crowding due to the star nature of the copolymer in BA(DBSA) complex led to lower aggregation number within cylindrical micelles and resulted in smaller interdomain distance.

On heating the SAXS intensity profile of BA(DBSA) complex showed a sharp change above 160 °C. The intensities of the peaks at both low and high q dropped

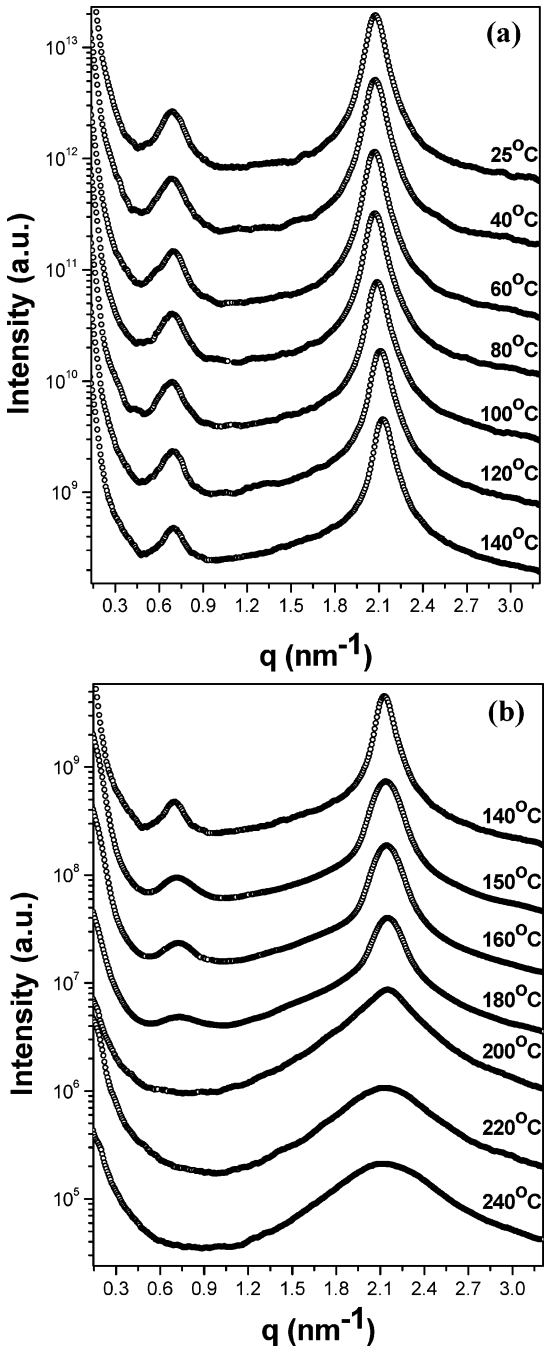

Figure 10. Temperature-dependent SAXS intensity profiles of BA(DBSA) comb−coil complex collected in situ from (a) 25 to 160 °C and (b) 160 to 240 °C in a heating cycle.

significantly above 150 °C, signaling the onset of ODT in the complex. The ODT observed from SAXS was in parallel with that observed from POM (see Supporting Information). The T_{ODT} of both large- and small-scale structure were further determined from the corresponding I_m^{-1} vs T^{-1} plots, as shown in Figure 11. Significant drops in intensities of the scattering peaks corresponding to the larger- and smaller-scale structure can be clearly observed near 160 °C. This indicated that the disordering of block copolymer microdomains occurred almost simultaneously with that of the P2VP(DBSA) lamellar structure. More specifically, the disruption of the copolymer domains occurred first, and this process induced disordering of the lamellar mesophase. This was in sharp contrast to that observed in LA(DBSA) complex where disordering of the P2VP(DBSA) lamellar

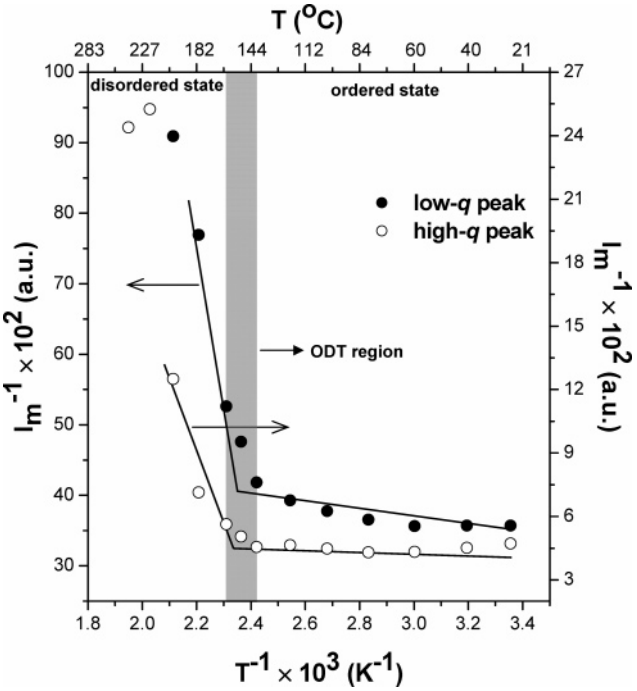

Figure 11. I_m^{-1} vs T^{-1} plots for estimating the T_{ODT}'s of the larger-scale structure formed by copolymer domains and the smaller-scale structure formed by P2VP(DBSA) comb blocks in the BA(DBSA) complex.

mesophase preceded that of the larger-scale copolymer domain structure.

It is also interesting to note that T_{ODT}'s of both the larger and smaller structures in BA(DBSA) comb−coil complex were significantly lower than those in the LA(DBSA) complex despite of the fact that T_{ODT}'s of neat LA and BA copolymers were almost the same. Moreover, the T_{ODT} of the copolymer domains in the BA(DBSA) complex was virtually the same as that of neat BA. The chain-crowding effect responsible for lowering the T_{ODT} of neat BA copolymer might also dominate the disordering in the BA(DBSA) complex. As can be observed from Figure 6b, for accommodating the longer free PS chains (shown in gray) within the PS cylindrical microdomains without crowding the junction point region, the shorter PS chains (shown in dark) of the diblock arm should also stretch significantly normal to the domain interface. The loss of conformational entropy due to stretching of the PS chains again dominated the free energy of the system and led to the disordering of large-scale copolymer domains at the temperature comparable to the T_{ODT} of neat BA. The disordering of the copolymer domains naturally disrupted the lamellar mesophase organized by the comb blocks to allow mixing between the PS and P2VP(DBSA) blocks.

Conclusions

The effect of block copolymer molecular architecture on the microphase separation behavior in supramolecular comb−coil complexes has been studied using the complex of DBSA with a $(PS\text{-}b\text{-}P2VP)_5PS_5$ block-arm star copolymer. Despite the complex chain architecture, $(PS\text{-}b\text{-}P2VP)_5(PS)_5$(DBSA) comb−coil complex exhibited hierarchical structure similar to that observed in the linear PS-*b*-P2VP(DBSA) complex. However, the chain-crowding effect at the star junction point together with the peculiar architecture of the $(PS\text{-}b\text{-}P2VP)_5PS_5$ star copolymer, where the length of free PS arms was

significantly greater than the PS chains in the diblock arms, drastically influenced its ordered-state morphology and ODT in both neat and complex state. In contrast to the linear PS-*b*-P2VP(DBSA) complex where the T_{ODT} of the larger-scale copolymer domain increased significantly compared to that of neat PS-*b*-P2VP, the T_{ODT} of the copolymer domain structure in $(PS\text{-}b\text{-}P2VP)_5(PS)_5$-(DBSA) complex remained virtually unaffected. To accommodate the longer free PS chains in star copolymer complex without significantly crowding the junction point, the short PS chains of the diblock arms also stretched normal to the domain interface and hence resulted in an entropic loss. At higher temperatures this entropic loss dominated the free energy landscape, and hence the system favored the disordered state despite the influence of the lamellar mesophase of the comb blocks. This chain crowding effect also explained the proximity of the T_{ODT} of neat $(PS\text{-}b\text{-}P2VP)_5(PS)_5$ block−arm star copolymer to that of neat linear PS-*b*-P2VP, although the T_{ODT} of simple $(AB)_n$ type of star copolymer was reported to be higher than that of linear AB copolymer. Furthermore, the star nature of the copolymer led to a lower aggregation number of macromolecules within the cylindrical microdomains of the $(PS\text{-}b\text{-}P2VP)_5(PS)_5$(DBSA) complex; consequently, the primary scattering maximum related to the characteristic interdomain spacing of the copolymer domains in $(PS\text{-}b\text{-}P2VP)_5(PS)_5$(DBSA) complex showed a significant high-q shift in the SAXS profile compare to that associated with the neat $(PS\text{-}b\text{-}P2VP)_5PS_5$.

Acknowledgment. We gratefully acknowledge financial support from the National Science Council under Contract NSC94-2216-E-007-039.

Supporting Information Available: Temperature-dependent POM micrographs, Fourier transform infrared (FTIR) spectra, and synchrotron SAXS profile of the LA(DBSA) complex. This material is available free of charge via the Internet at http://pubs.acs.org.

References and Notes

(1) Leibler, L. *Macromolecules* **1980**, *13*, 1602.
(2) Bates, F. S.; Fredrickson, G. H. *Annu. Rev. Phys. Chem.* **1990**, *41*, 525.
(3) Chen, J. T.; Thomas, E. L.; Ober, C. K.; Mao, G.-P. *Science* **1996**, *273*, 343.
(4) Hamley, I. W. *The Physics of Block Copolymers*; Oxford University Press: New York, 1998.
(5) Muthukumar, M.; Ober, C. K.; Thomas, E. L. *Science* **1997**, *277*, 1225.
(6) Bates, F. S.; Fredrickson, G. H. *Phys. Today* **1999**, *52*, 32.
(7) Lodge, T. P. *Macromol. Chem. Phys.* **2003**, *204*, 265.
(8) Park, C.; Yoon, J.; Thomas, E. L. *Polymer* **2003**, *44*, 6725.
(9) Hadjichristidis, N.; Pispas, S.; Floudas, G. *Block Copolymers: Synthetic Strategies, Physical Properties, and Applications*; Wiley-Interscience: New York, 2003.
(10) Plate', N. A.; Shibaev, V. P. *Comb-Shaped Polymers and Liquid Crystals*; Plenum Press: New York, 1987.
(11) Antonietti, M.; Conrad, J.; Thünemann, A. *Macromolecules* **1994**, *27*, 6007.
(12) Ikkala, O.; Ruokolainen, J.; ten Brinke, G.; Torkkeli, M.; Serimaa, R. *Macromolecules* **1995**, *28*, 7088.
(13) Ruokolainen, J.; ten Brinke, G.; Ikkala, O.; Torkkeli, M.; Serimaa, R. *Macromolecules* **1996**, *29*, 3409.
(14) ten Brinke, G.; Ikkala, O. *Trends Polym. Sci.* **1997**, *5*, 213.
(15) Ruokolainen, J.; Mäkinen, R.; Torkkeli, M.; Mäkelä, T.; Serimaa, R.; ten Brinke, G.; Ikkala, O. *Science* **1998**, *280*, 557.
(16) Ikkala, O.; Knaapila, M.; Ruokolainen, J.; Torkkeli, M.; Serimaa, R.; Jokela, K.; Horsburgh, L.; Monkman, A.; ten Brinke, G. *Adv. Mater.* **1999**, *11*, 1206.
(17) Chen, H. L.; Hsiao, M. S. *Macromolecules* **1999**, *32*, 2967.
(18) Ruokolainen, J.; Eerikainen, H.; Torkkeli, M.; Serimaa, R.; Jussila, M.; Ikkala, O. *Macromolecules* **2000**, *33*, 9272.
(19) Hartikainen, J.; Lahtinen, M.; Torkkeli, M.; Serimaa, R.; Valkonen, J.; Rissanen, K.; Ikkala, O. *Macromolecules* **2001**, *34*, 7789.
(20) Kato, T.; Mizoshita, N.; Kanei, K. *Macrol. Rapid Commun.* **2001**, *22*, 797.
(21) Ikkala, O.; ten Brinke, G. *Science* **2002**, *295*, 2407.
(22) Chen, H. L.; Ko, C. C.; Lin, T. L. *Langmuir* **2002**, *18*, 5619.
(23) Nandan, B.; Chen, H. L.; Liao, C. S.; Chen, S. A. *Macromolecules* **2004**, *37*, 9561.
(24) Ruokolainen, J.; Saariaho, M.; Ikkala, O.; ten Brinke, G.; Thomas, E. L.; Torkkeli, M.; Serimaa, R. *Macromolecules* **1999**, *32*, 1152.
(25) Ruokolainen, J.; ten Brinke, G.; Ikkala, O. *Adv. Mater.* **1999**, *11*, 777.
(26) Ruotsalainen, T.; Torkkeli, M.; Serimaa, R.; Mäkelä, T.; Mäki-Ontto, R.; Ruokolainen, J.; ten Brinke, G.; Ikkala, O. *Macromolecules* **2003**, *36*, 9437.
(27) Polushkin, E.; Alberda van Ekenstein, G.; Dolbnya, I.; Bras, W.; Ikkala, O.; ten Brinke, G. *Macromolecules* **2003**, *36*, 1421.
(28) Alberda van Ekenstein, G.; Polushkin, E.; Nijland, H.; Ikkala, O.; ten Brinke, G. *Macromolecules* **2003**, *36*, 3684.
(29) Valkama, S.; Ruotsalainen, T.; Kosonen, H.; Ruokolainen, J.; Torkkeli, M.; Serimaa, R.; ten Brinke, G.; Ikkala, O. *Macromolecules* **2003**, *36*, 3986.
(30) Kosonen, H.; Valkama, S.; Ruokolainen, J.; Torkkeli, M.; Serimaa, R.; ten Brinke, G.; Ikkala, O. *Eur. Phys. J. E* **2003**, *10*, 69.
(31) Valkama, S.; Kosonen, H.; Ruokolainen, J.; Haatainen, T.; Torkkeli, M.; Serimaa, R.; ten Brinke, G.; Ikkala, O. *Nat. Mater.* **2004**, *3*, 872.
(32) Ikkala, O.; ten Brinke, G. *Chem. Commun.* **2004**, *19*, 2131.
(33) Bondzic, S.; de Wit, J.; Polushkin, E.; Schouten, A. J.; ten Brinke, G.; Ruokolainen, J.; Ikkala, O.; Dolbnya, I.; Bras, W. *Macromolecules* **2004**, *37*, 9517.
(34) Tsao, C.-S.; Chen, H.-L. *Macromolecules* **2004**, *37*, 8984.
(35) ten Brinke, G.; Ikkala, O. *Chem. Rec.* **2004**, *4*, 219.
(36) Polushkin, E.; Bondzic, S.; de Wit, J.; Alberda van Ekenstein, G.; Dolbnya, I.; Bras, W.; Ikkala, O.; ten Brinke, *Macromolecules* **2005**, *38*, 1804.
(37) Olvera de la Cruz, M.; Sanchez, I. C. *Macromolecules* **1986**, *19*, 2501.
(38) Dobrynin, A. V.; Erukhimovich, I. Ya. *Macromolecules* **1993**, *26*, 276.
(39) Milner, S. T. *Macromolecules* **1994**, *27*, 2333.
(40) Olmsted, P. D.; Milner, S. T. *Macromolecules* **1998**, *31*, 4011.
(41) Floudas, G.; Hadjichristidis, N.; Iatrou, H.; Pakula, T.; Fischer, E. W. *Macromolecules* **1994**, *27*, 7735.
(42) Floudas, G.; Pispas, S.; Hadjichristidis, N.; Pakula, T.; Erukhimovich, I. *Macromolecules* **1996**, *29*, 4142.
(43) Floudas, G.; Paraskeva, S.; Hadjichristidis, N.; Fytas, G.; Chu, B.; Semenov, A. N. *J. Chem. Phys.* **1997**, *107*, 5502.
(44) Floudas, G.; Hadjichristidis, N.; Iatrou, H.; Avgeropoulos, A.; Pakula, T. *Macromolecules* **1998**, *31*, 6943.
(45) Buzza, D. M. A.; Hamley, I. W.; Fzea, A. H.; Moniruzzaman, M.; Allgaier, J. B.; Young, R. N.; Olmsted, P. D.; McLeish, T. C. B. *Macromolecules* **1999**, *32*, 7483.
(46) Ishizu, K.; Uchida, S. *Prog. Polym. Sci.* **1999**, *24*, 1439.
(47) Grayer, V.; Dormidontova, E. E.; Hadziioannou, G.; Tsitsilianis, C. *Macromolecules* **2000**, *33*, 6330.
(48) Matsen, M. W.; Gardiner, J. M. *J. Chem. Phys.* **2000**, *113*, 1673.
(49) Zhu, Y.; Gido, S. P.; Moshakou, M.; Iatrou, H.; Hadjichristidis, N.; Park, S.; Chang, T. *Macromolecules* **2003**, *36*, 5719.
(50) Nandan, B.; Lee, C.-H.; Chen, H.-L.; Chen, W.-C, Hashimoto, T., manuscript in preparation.
(51) Yang, C. C.; Wu, P.-T.; Chen, W.-C.; Chen, H.-L. *Polymer* **2004**, *45*, 5691.
(52) Tsitsilianis, C.; Voulgaris, D. *Macromol. Chem. Phys.* **1997**, *198*, 997 and references therein.
(53) Porod, G. *Kolloid-Z.* **1951**, *124*, 83.
(54) Porod, G. *Kolloid-Z.* **1952**, *125*, 51.
(55) Ruland, W. J. *J. Appl. Crystallogr.* **1971**, *4*, 70.
(56) de Gennes, P. G. *Scaling Concepts in Polymer Physics*; Cornell University Press: Ithaca, NY, 1985.
(57) Ogawa, T.; Sakamoto, N.; Hashimoto, T.; Han, C. D.; Baek, D. M. *Macromolecules* **1996**, *29*, 2113.
(58) Hashimoto, T.; Ijichi, Y.; Fetters, L. J. *J. Chem. Phys.* **1988**, *89*, 2463.
(59) Mountrichas, G.; Mpiri, M.; Pispas, S. *Macromolecules* **2005**, *38*, 940.

MA051448T